Anal. Chem. **2006,** *78,* 44−51

Articles

Hadamard Transform Ion Mobility Spectrometry

Brian H. Clowers,*,†,‡ William F. Siems,† Herbert H. Hill,†,‡ and Steven M. Massick*,§

Department of Chemistry and Center for Multiphase Environmental Research, Washington State University, Pullman, Washington 99164, and Southwest Sciences Inc., Santa Fe, New Mexico 87505

Traditionally, the spectrum acquired using ion mobility spectrometry (IMS) is an average of multiple experimental cycles. Each cycle is initiated by passing a short burst of ions into a drift tube containing a homogeneous electric field. Prior to starting the subsequent cycle, all ions in the system must arrive at the detector or spectral overlap may occur. To maximize resolution, the ion pulse admitted to the drift tube is small in relation to the total scan time with the unfortunate consequence of an inherently low duty cycle (∼1%). Offering an improved SNR through a 50% duty cycle, the Hadamard transform (HT) applied to ion mobility spectrometry represents a fresh alternative to signal-averaged data acquisition. Initial results from measurements of amphetamine and cytochrome *c* samples indicate a 2−10-fold increase in SNR for the HT-IMS technique with no reduction in resolution.

Ion mobility spectrometry (IMS), a postionization gas-phase separation technique, has been used for the rapid detection of explosives, narcotics, and chemical warfare agents.[1−5] The evolution of IMS has progressed from a technique primarily applied to gas-phase samples to liquid- and solid-phase samples through the coupling of electrospray ionization (ESI)[6] and matrix-assisted laser desorption/ionization.[7] From proteins to carbohydrates, these ionization sources when coupled with IMS have allowed the gas-phase chemistries of biologically relevant compounds to be probed. When combined with mass spectrometry and computational modeling, IMS has been integral in the elucidation of gas-phase conformations of complex systems.[8−12]

IMS experiments are conducted with a drift tube containing a homogeneous gas held at a constant pressure. Pulses of ions are introduced into the drift tube region where separation occurs according to the magnitude of the applied electric field, the frequency of ion−neutral interactions, and the charge and collision cross section of each ion. Typically, IMS instruments utilize a continuous ionization source, e.g., ^{63}Ni or ESI, thereby necessitating the use of an ion gate such as a Bradbury−Nielson (B−N) gate. In an IMS experiment, a pulse applied to the B−N gate initiates the experimental cycle by admitting a discrete packet of ions into the drift region. To avoid spectral overlap, the drift−time measurement of each ion packet must be completed prior to initiation of the next sequence. The B−N gate pulse is often small (250 μs) compared to that of the total experimental sequence (25 ms), resulting in an IMS experimental duty cycle of ∼1% with the bulk of the sample ions being neutralized on the ion gate. Furthermore, since increasing the duty cycle by lengthening the ion gate pulse degrades the resolution, one must often sacrifice analytical throughput or overall sensitivity in order to meet resolution requirements.

Ion trapping[13] experiments have been conducted to overcome the inherently low duty cycle of IMS coupled with continuous ion sources; however, this adds considerable complexity to the method. Indeed, most implementations of IMS still rely on signal averaging (SA) of multiple, low-duty cycle drift spectra. Recently, the application of Hadamard-type signal multiplexing has been successfully applied to a variety of pulsed separation techniques such as time-of-flight mass spectrometry[14,15] and capillary electrophoresis.[16] First applied to optical spectrometers, signal multiplexing by means of the application of Hadamard-type transforms

* To whom correspondence should be addressed. E-mail: bhclowers@yahoo.com. Tel: (509) 335-7752. Fax: (509) 335-7636. E-mail: smassick@swsciences.com. Tel: (505) 984-1322. Fax: (505) 98-9230.

† Department of Chemistry, Washington State University.

‡ Center for Multiphase Environmental Research, Washington State University.

§ Southwest Sciences Inc.

(1) Ewing, R. G.; Atkinson, D. A.; Eiceman, G. A.; Ewing, G. J. *Talanta* **2001**, *54* (3), 515−29.

(2) Asbury, G. R.; Klasmeier, J.; Hill, H. H., Jr. *Talanta* **2000**, *50* (6), 1291−8.

(3) Matz, L. M.; Hill, H. H., Jr. *Anal. Chem.* **2001**, *73* (8), 1664−9.

(4) Steiner, W. E.; Clowers, B. H.; Matz, L. M.; Siems, W. F.; Hill, H. H., Jr. *Anal. Chem.* **2002**, *74* (17), 4343−52.

(5) Asbury, G. R.; Wu, C.; Siems, W. F.; Hill, H. H., Jr. *Anal. Chim. Acta* **2000**, *404* (2), 273−83.

(6) Wittmer, D.; Chen, Y. H.; Luckenbill, B. K.; Hill, H. H., Jr. *Anal. Chem.* **1994**, *66* (14), 2348−55.

(7) Gillig, K. J.; Ruotolo, B.; Stone, E. G.; Russell, D. H.; Fuhrer, K.; Gonin, M.; Schultz, A. J. *Anal. Chem.* **2000**, *72* (17), 3965−71.

(8) Henderson, S. C.; Valentine, S. J.; Counterman, A. E.; Clemmer, D. E. *Anal. Chem.* **1999**, *71* (2), 291−301.

(9) Gidden, J.; Baker, E. S.l; Ferzoco, A.; Bowers, M. T. *Inter. J. Mass Spectrom.* **2005**, *240* (3), 183−93.

(10) Barran, P. E.; Polfer, N. C.; Campopiano, D. J.; Clarke, D. J.; Langridge-Smith, P. R. R.; Langley, R. J.; Govan, J. R. W.; Maxwell, A.; Dorin, J. R.; Millar, R. P.; Bowers, M. T. *Int. J. Mass Spectrom.* **2005**, *240* (3), 273−84.

(11) Hill, H. H., Jr.; Hill, C. H.; Asbury, G. R.; Wu, C.; Matz, L. M.; Ichiye, T. *Inter. J. Mass Spectrom.* **2002**, *219* (1), 23−37.

(12) Leavell, M. D.; Gaucher, S. P.; Leary, J. A.; Taraszka J. A.; Clemmer, D. E. *J. Am. Soc. Mass. Spectrom.* **2002**, *13* (3), 284−93.

(13) Henderson, S. C.; Valentine, S. J.; Counterman, A. E.; Clemmer, D. E. *Anal. Chem.* **1999**, *71* (2), 291−301.

(14) Brock, A.; Rodriguez, N. Zare, R. N. *Anal. Chem.* **1998**, *70* (18), 3735−41.

(15) Brock, A.; Rodriguez, N.; Zare, R. N. *Rev. Sci. Instrum.* **2000**, *71* (3), 1306−18.

(16) Kaneta, T.; Yamaguchi, Y.; Imasaka, T. *Anal. Chem.* **1999**, *71* (23), 5444−6.

10.1021/ac050615k CCC: $33.50
Published on Web 11/25/2005

provides the benefits of an increased duty cycle and improved signal-to-noise ratio (SNR) when compared to signal averaging techniques.[17] The Hadamard transform (HT) utilizes a binary series, in this case, a series of open and close pulses applied to the B−N gate, followed by deconvolution to realize the multiplexing advantage.[18] Specifically, for our implementation of Hadmard transform IMS (HT-IMS), the B−N ion gate is modulated in accordance with a known series of pulses, effectively producing many ion packets that intermingle in the separation region. The signal acquired during an HT-IMS experiment is thus a superposition of drift spectra, and according to the properties of Hadamard transforms, the duty cycle of IMS is increased to 50%. To retrieve ion mobility drift spectra, the superimposed signal is deconvoluted with the inverse of the applied Hadamard transform.[18]

Increases in IMS duty cycle through multiplexing have been achieved using Fourier transform (FT) methods.[19,20] However, unlike HT-IMS, implementation of FT-IMS requires the operation of a second B−N ion gate (implemented either physically or through software).[21] Because the Fourier transform method applied to IMS is sensitive to changes in the efficiency of the ion gate high pulse frequencies, the application of an apodization function is necessary to avoid baseline artifacts in the retrieved drift spectra.[22] In contrast, adapting an IMS system for Hadamard-type multiplexing requires no physical instrument modifications and, in comparison to the Fourier method, implementing the Hadamard algorithm is less computationally intensive. This work communicates the evaluation of Hadamard transform ion mobility spectrometry and its potential to increase experimental signal-to-noise ratio.

THEORETICAL BACKGROUND

Hadamard Transform. Given the number of highly detailed reviews and descriptions available regarding Hadamard transform methods, only a brief outline of the Hadamard transform is presented.[18,23,24] Traditionally, a data set acquired using conventional signal-averaged IMS (SA-IMS) methods contains a fixed number of data points that individually possess a degree of error. In contrast, the error associated with a data point acquired using multiplexing methods, following deconvolution, is distributed throughout the acquired data set. More specifically, for the measurement of N spectral elements, e.g., the ion signal at N time intervals, the error associated with the measurement of any one element can be reduced by measuring N combinations of multiple elements in a fashion that allows the determination of the values of the individual elements. The measurements η_i are related to the elements ψ_i by a matrix transformation, where η and ψ are vectors representing the multiplexed ion signal measurement and the mobility spectrum, respectively, and $\boldsymbol{S}_N$ is a $N \times N$ matrix that describes the measurement design.

$$\eta = S_N \cdot \psi \tag{1}$$

For example, the slit of a monochromator may be replaced by a mask containing many slits, or in the case of IMS, the single pulse ion packet may be replaced by multiple overlapping ion packets formed by a sequence of pulses applied to an ion gate. Hadamard transform theory provides measurement designs for the determination of ψ that are optimized for SNR enhancement.[18]

Hadamard transforms apply to measurements where the individual elements ψ_i can be added and subtracted to form the multiplexed signal. Thus, when displayed in matrix form, the Hadamard transform is composed of a series of ones and negative ones. However, in circumstances where the spectral elements can only be added or omitted, e.g., the operation of an ion gate in an IMS system, the Hadamard matrix is modified to produce a Simplex matrix composed of zeros and ones. The ones and zeros of the Simplex code represent the opening and closing of the ion gate, respectively. Simplex matrices are easily derived from Hadamard matrices by deleting the first row and column of the Hadamard matrix and replacing each 1 value with 0 and each −1 value with 1.[18] With knowledge of the order in which the ones and zeros of the Simplex matrix are applied to the ion gate, i.e., the modulation sequence, the resulting multiplexed ion signal may be deconvoluted to produce a mobility spectrum that displays ion current as a function of drift time.

The Simplex-type matrices used in this work were derived from simple binary operations that generate maximum length, pseudorandom sequences (m-sequences). These recurrent sequences can be generated by known binary operations with periods $n = 2^m - 1$, where m is the length of a bit shift operation.[18] For example, an m-sequence of $n = 255$ (a S_{255} transform) is generated by an 8-bit shift operation, and upon sweeping an 8-element window along this recurrent sequence, every binary number from 1 to 255 will be observed once in a "pseudorandom" order. The length of the bit shift operation is one of three parameters that govern the performance of the HT-IMS. The second and third parameters are the time resolution, i.e., the modulation rate of the m-sequence and, most importantly, the performance of the ion gate. Multiplexed ion signals corresponding to entire m-sequences were also coaveraged during HT-IMS operation.

EXPERIMENTAL SECTION

Chemicals and Reagents. Standard sample solutions were prepared in 1-mL aliquots of a solvent comprising a 75:25 v/v mixture of water (18.1 MΩ cm^{-1}) and methyl alcohol (Fisher Scientific) with an additional 1 μL of 6 M acetic acid for every 1 mL of solvent. Sample solutions of amphetamine (MW 135.2, Sigma-Aldrich) were prepared and analyzed at concentrations of 20 ppm (148 nmol/mL). Cytochrome *c* (Sigma, St. Louis, MO) samples were analyzed at a concentration of 100 nmol/mL.

Electrospray Ionization Atmospheric Pressure Ion Mobility Spectrometer (APIMS). SA-IMS and HT-IMS experiments were conducted using an electrospray ionization APIMS (Figure 1) constructed at Washington State University. This instrument was composed of the following components: (1) ESI source; (2)

(17) Larson, N. M.; Crosmun, R.; Talmi, Y. *Appl. Opt.* **1974**, *13* (11), 2662−8.
(18) Harwit, M.; Sloane, N. J. A. *Hadamard Transform Optics*; Academic Press: New York, 1979; pp 1−19, 200−223.
(19) Knorr, F. J.; Eatherton, R. L.; Siems, W. F.; Hill, H. H., Jr. *Anal. Chem.* **1985**, *57* (2), 402−6.
(20) Chen, Y. H.; Siems, W. F.; Hill, H. H., Jr. *Anal. Chim. Acta* **1996**, *334* (1−2), 75−84.
(21) Tarver, E.; Stamps, J. F.; Jennings, R. T.; Siems, W. F. *Int. J. Ion Mobility Spectrom.* **2001**, *4* (1), 57−9.
(22) St. Louis, R. H.; Siems, W. F.; Hill, H. H., Jr. *Anal. Chem.* **1992**, *64* (2), 171−7.
(23) Fernandez, F. M.; Vadillo, J. M.; Engelke, F.; Kimmel, J. R.; Zare, R. N.; Rodriguez, N.; Wetterhall, M.; Markides, K. *J. Am. Soc. Mass Spec.* **2001**, *12* (12), 1302−11.
(24) Wilhelmi, G.; Gompf, F. *Nucl. Instrum. Methods* **1970**, *81*, 36−44.

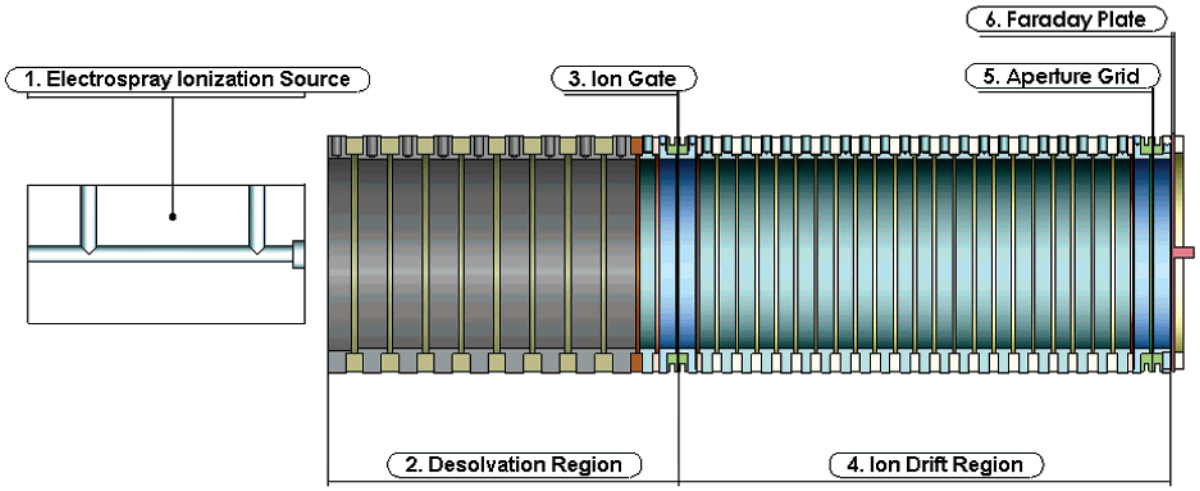

Figure 1. Electrospray ionization atmospheric pressure ion mobility spectrometer. This instrument is composed of the following parts: (1) electrospray ionization source; (2) desolvation region; (3) Bradbury−Nielson ion gate; (4) counterflow ion drift region; (5) aperture grid; and (6) Faraday plate.

heated AP desolvation region; (3) Bradbury−Nielson ion gate; (4) counterflow AP drift region; (5) aperture grid; (6) and Faraday detection plate. Each standard sample solution was delivered to the ESI source at 3 μL/min through PEEK tubing (Upchurch Scientific, Oak Harbor, WA) connected to a 175 μm:75 μm o.d.: i.d. polyimide silica capillary (PolyMicro Technologies, Phoenix, AZ) through a zero dead volume metal union (Valco Instruments, Houston, TX). The electric connection for the custom-built ESI unit was maintained at 11.6 kV, ~3.0 kV greater than the potential of the entrance to the desolvation region. A countercurrent flow (1 L/min) of heated nitrogen drift gas (175 °C and 690 Torr) desolvated ionized sample molecules prior to ion gating. The B−N ion gate consists of a parallel arrangement of alloy 46 stainless steel wires (76-μm diameter) separated by 0.64 mm that are supported by 50-mm-i.d. alumina rings. Electrical connections to the B−N gate establish two isolated sets of interleaved wires. A potential difference applied to adjacent wires within the B−N ion gate prevents ions from entering the drift region. The B−N gate was held at 7680 V, and the potential difference of the interleaved wire sets was 40 V in the closed state. The ion drift region of the IMS system consists of a series of stacked stainless steel rings (47-mm i.d.) that are insulated by alumina spacers and connected in series by 1-MΩ precision resistors (Caddock Electronics, Riverside, CA). The resistive voltage divider defines the potentials of the 17.4-cm column of stacked rings in the drift region to produce a uniform electric field (440 V/cm). For these experiments, the sole purpose of the aperture grid was to shield the drift region from the Faraday plate potential. The Faraday plate current was amplified by a Keithely 427 current amplifier (Keithley Instruments, Cleveland, OH) operated with a rise time of 30 μs and gain of 10^8 for all SA-IMS and HT-IMS experiments.

Signal-Averaging Pulse Generation and Acquisition System. Signal-averaged spectra were acquired using a PCI-MIO-16XE-10 data acquisition card (National Instruments, Austin, TX) equipped with a 16-bit analog-to-digital (A/D) converter. Experimental timings and signal acquisition were controlled using custom software developed with LabVIEW 6.1 (National Instruments, Austin, TX). The pulse output for the B−N ion gate, in the form of a transistor−transistor logic (TTL) pulse from the PCI card, was relayed to a custom ion gate controller. This controller simultaneously references the voltage applied to the drift tube and outputs the profile of the TTL pulse at voltage levels appropriate for opening and closing of the ion gate. Pulses for the atmospheric pressure SA-IMS experiments ranged from 100 to 300 μs in length. Two 2 × 50 Ω, 2 W attenuators (Tektronix, Beaverton, OR) were attached to the inputs of the data acquisition boards for both the SA- and HT-IMS experiments. The ion signal collection rate was 40 kHz for a drift time window of 25 ms. Multiple drift spectra were averaged and recorded to an output file.

Hadamard Sequence Generation and Acquisition System. To easily demodulate the multiplexed ion signal and retrieve a mobility spectrum. it is necessary to precisely synchronize the signal acquisition to the output of the Hadamard modulation sequence. For this purpose, a dedicated digital signal processing (DSP) electronics board was used for both the Hadamard sequence output and ion signal acquisition. A combination of a programmable DSP evaluation module from Spectrum Digital (model DSK6713, Stafford, TX) and an accessory board with synchronous analog-to-digital (A/D) and digital-to-analog (D/A) conversion capabilities (AED101, SignalWare, Colorado Springs, CO) were selected for the HT-IMS experiments. Code Composer Studio version 2.20 (Texas Instruments Inc. Stafford, TX) was used for C language programming of the DSK6713 and also for data transfer from the DSK6713 to a laptop computer. The AED101 board is equipped with two 12-bit A/D converters and two 12-bit D/A converters operated by a field-programmable gate array (FPGA). Custom FPGA programming synchronized the A/D and D/A conversions, and provided data compression by reducing the resolution of the A/D data to 8-bit values and the D/A data to 1-bit values. The maximum A/D sampling rate and D/A output rate of the DSP electronics is limited by data transfer from the AED101 to the DSK6713 and was determined to be 30 and 15 MHz, respectively. For these experiments, the A/D sampling rate was set to twice the modulation (D/A) rate to over sample the modulation sequence.

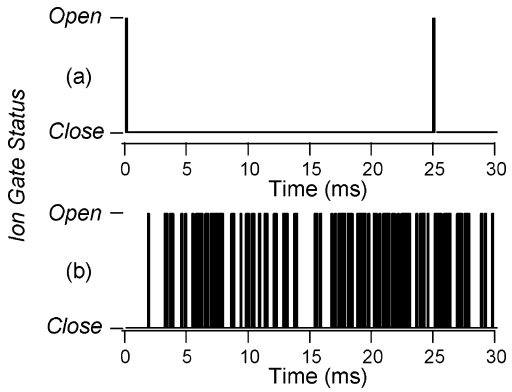

Figure 2. Comparison of the ion gate pulse sequences between the traditional signal averaged (a) and the Hadamard transform (b) modes of operation. While the duty cycle for the Hadamard sequence (S_{8191}, 150-μs pulse width) is ~50%, the duty cycle for a 40-Hz, 150-μs pulse width signal averaging approach is 0.6%. For the purpose of display, only 2.4% of the complete Hadamard sequence is shown.

The DSK6713 was programmed to allow the user to select m-sequences periods ranging from 15 to 1 048 575 corresponding to 4−20-bit shift lengths. The FPGA contains two 511 element 32 bit FIFO buffers for the A/D input and the D/A output. For long *m*-sequences and averages of multiple *m*-sequences, the D/A FIFO is continually refreshed immediately following A/D data transfers to permit continuous operation with a valid modulation sequence output. The recorded ion signal was transferred directly to memory on the DSK6713 where it was signal-averaged commensurate to the *m*-sequence length. The averaged multiplexed ion signal, thus obtained, was then transferred to a laptop computer for analysis. The gains of the input and output amplifiers on the AED101 were altered to match the requirements of the existing IMS ion gate and ion signal electronics. Switching between SA-IMS and HT-IMS operational modes simply required changing two BNC cable connections.

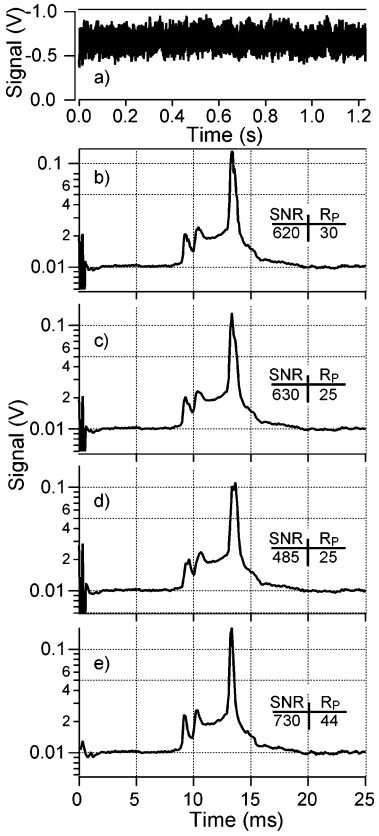

Figure 3. Deconvolution results using four different methods. Trace a represents the raw multiplexed amphetamine ion signal acquired at 75-μs intervals with a 150-μs modulation resolution S_{8191} transform. Traces b−e resulted from the inverse Hadamard transform of trace a using the data processing methods as follows: (b) all points processed; (c) deconvolution of the average of every two data points; (d) deconvolution of data points that coincide with the HT modulation pulse clock; (e) deconvolution of data points offset by 75 μs from the HT modulation pulse clock.

RESULTS AND DISCUSSION

Application of the Hadamard transform to time-of-arrival measurements requires that the modulation resolution and *m*-sequence length be selected such that the slowest ion drift time is less than the period of an entire *m*-sequence. For example, the temporal window common for mobility measurements of small ions is 25 ms, and to match this 25-ms temporal window with a 13-bit *m*-sequence (S_{8191}), a 3-μs modulation resolution is required. However, given the comparatively slow rate of ion migration through the B−N ion gate, such high rates of ion gate modulation are beyond the abilities of a B−N ion gate operated at atmospheric pressure. Consequently, we applied ion gate modulations with longer time resolutions, typically 150 μs, that resulted in *m*-sequence periods far in excess of the ion drift times, e.g., 1.23 s for a S_{8191} transform. The performance of the B−N gate ultimately limits the effective sampling rate of the HT-IMS drift spectra since the resolution of the deconvoluted drift spectra is equal to the time resolution of the modulation. A comparison of the SA-IMS and HT-IMS pulse sequences (Figure 2) illustrates the significant differences between the two experimental designs and, in the case of the HT-IMS pulse sequence, the occurrence of both short and long ion pulses.

Hadamard Signal Processing. Although the DSP electronics are capable of performing the deconvolution, for these initial studies, the recorded multiplexed ion signals were instead transferred from the DSK6713 controller board to a personal computer where the deconvolutions were performed in Igor Pro, version 5.0. Shown in Figure 3a is the complete multiplexed ion signal from the measurement of a 20 ppm solution of amphetamine. The ion gate was modulated according to a S_{8191} transform with a modulation resolution of 150 μs, and the data are an average of 16 complete *m*-sequences. Several different methods of applying the inverse Hadamard transform on the recorded ion signal were evaluated. Since the HT-IMS ion signal was acquired at twice the rate of gate modulation, it is necessary to first halve the number of points by either averaging or parsing the ion signal data set or alter the *m*-sequence, before deconvolution of the multiplexed ion signal.

The HT-IMS spectrum in Figure 3b was obtained by deconvolution of the multiplexed ion signal with a doubled *m*-sequence. Rather than combining two consecutive *m*-sequences, "doubling" entails that each *m*-sequence element be immediately repeated. For example the sequence 010110 becomes 001100111100 upon doubling. The strong ion signal observed at 13.35 ms is due to amphetamine, with a reduced mobility value (K_o) of 1.65 cm^2/V·s.[26] The smaller peaks observed at earlier drift times correspond to solvent ions. It is not necessary to deconvolute the entire 1.23-s

modulation period since deconvolution of 170 points (25.5 ms) is sufficient to retrieve the entire mobility spectrum for amphetamine. Extending the deconvolution to the full modulation period reveals a ±1-mV baseline with several small spikes at times well outside the 25-ms window. The signal at $t = 0$ is due to electromagnetic interference from the switching of the ion gate pulse electronics. This ion gate pulse signal is common for data collected with a Faraday plate and is also observed in SA-IMS drift spectra. Notably, the amphetamine peak in Figure 3b has an irregular peak shape with a small shoulder located at a slightly longer drift time. The HT-IMS spectrum shown in Figure 3c that was obtained by averaging two successive points to halve the multiplexed ion signal data set also displays an irregular, broadened amphetamine peak.

The HT-IMS spectra obtained by parsing the multiplexed ion signal are shown in Figure 3d and e. The spectrum in Figure 3d was obtained by deconvolution of only the ion signal points that were coincident with the D/A clock that controls the open or closed state of the B−N gate. Figure 3e shows the deconvolution of the remaining half of the ion signal that were sampled at least 75 μs from any changes in the ion gate state, i.e., 180° out of phase with the D/A clock. Notably, the ion gate pulse signal at $t = 0$ is nearly absent in spectrum in Figure 3e, and the amphetamine peak shape is not degraded, unlike the spectra obtained by the other deconvolution methods. The ion gate pulse signal can be considered a zero drift time spectral element, so it is not surprising that it is attenuated by the deconvolution of only ion signal recorded 75 μs afterward. However, the improved amphetamine peak shape in Figure 3e is not the related to the reduced gate pulse signal. The gate pulse signal was initially suspect since this signal occurs throughout the signal acquisition period in HT-IMS mode, and the possible effect of noise associated with the gate pulse signal upon the deconvoluted spectra was not clear. Simulations were performed where various amounts of the gate pulse signal as measured by SA-IMS were added or subtracted to the HT-IMS multiplexed ion signal in Figure 3a at points corresponding to the opening of the gate. Comparisons of the spectra obtained by deconvolutions of these modified data sets using the deconvolution method observed to produce split peaks (as in Figure 3d) demonstrated that the gate pulse signal near $t = 0$ varied strongly with the amount of correction; however, the amphetamine peak displayed no changes. Furthermore, in experiments where the potential difference applied to the B−N ion gate was increased and the intensity of the gate pulse signal was larger than the amphetamine ion signal, no increased broadening or splitting of the amphetamine peak occurred.

The cause of the degraded amphetamine peak shape in Figure 3b−d is related to the performance of the B−N ion gate, i.e., the ability of the B−N gate to admit ions into the drift region in a fashion that accurately reproduces the modulation sequence. The mathematics of the Hadamard transform assume the signal registered by the detector is a function of a perfect gating sequence; i.e., ideally ions would be instantaneously repelled and admitted to the drift region. Unfortunately, the depletion of ions near the B−N gate wires (in the closed state) causes a significant discrepancy between the applied pulse sequence and the actual

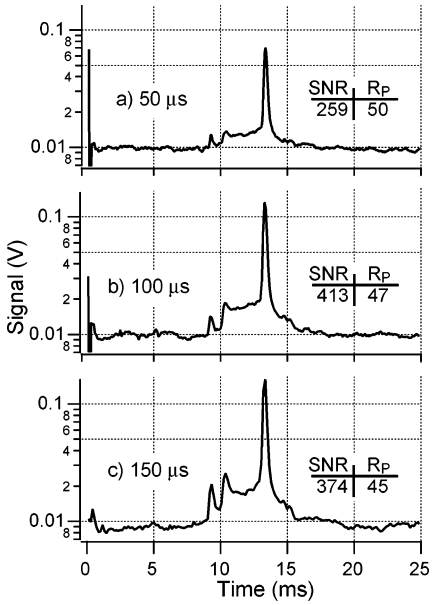

Figure 4. HT-IMS amphetamine spectra a−c representing the result of a S_{8191} modulation sequence acquired at modulation resolutions of 50, 100, and 150 μs, respectively. The spectra are deconvolutions of averages of the multiplexed ion signal of eight complete S_{8191} modulation sequences.

widths of ion packets introduced into the drift region. The Hadamard modulation contains periods of short open and close pulses that will be sensitive to the effects of gate depletion. Modulation defects are known to produce spurious peaks in the baseline as well as to reduce the SNR.[26,27] A modulation defect such as a delayed admittance of ions through the B−N gate can be corrected by varying the *m*-sequence used for deconvolution of the multiplexed ion signal. We performed additional simulations designed to mimic the effective performance of the B−N gate by varying the *m*-sequence elements that correspond to the leading edges of the ion gate open pulses to nonbinary values. The resulting spectra demonstrated that the split character of the amphetamine peak shape is related to this type of modulation defect. Although the application of this simple modification to the *m*-sequence was not sufficient to fully correct the distorted amphetamine peak shapes of Figure 3b−d, we conclude that ion gate response and ion depletion are relevant concerns and sources of spectral defects for HT-IMS operation.

The spectrum shown in Figure 3e represents the most favorable method of HT-IMS data processing. This method discards the multiplexed ion signal that is most affected by the nonideal performance of the B−N ion gate, i.e., the ion signal that does not fully reflect the Hadamard modulation sequence. The resulting drift spectra obtained in this manner are relatively free of spectral features due to modulation defects. Consequently, by sampling only ion signal delayed from any changes in the open or close state of the B−N gate, the effective performance of the B−N ion gate is maximized. Given the relative success of this method of data processing, all subsequent deconvolutions utilized this technique.

Effect of Hadamard Modulation Resolution. The amphetamine spectra shown in Figure 4a−c were acquired in HT-IMS

(25) Lawrence, A. H. *Anal. Chem.* **1986**, *58* (6), 1269−72.
(26) Tilotta, D. C.; Hammaker, R. M.; Fateley, W. G. *Appl. Opt.* **1987**, *26* (19), 4285−92.
(27) Tai, M. H.; Harwit, M.; Sloane, N. J. A. *Appl. Opt.* **1975**, *14* (11), 2678−86.

mode with a S_{8191} transform using modulation resolutions of 50, 100, and 150 μs, respectively. To evaluate these spectra, we calculate the SNR as the peak height divided by the standard deviation of the baseline between 20 and 25 ms. The Hadamard technique has a constant duty cycle of ~50%; therefore, it is interesting that the intensity of the amphetamine peak is noticeably attenuated at short modulation resolutions and this adversely affects the SNR. The reduced amphetamine peak intensity in Figure 4a results from nonideal performance of the B−N gate, albeit a different manifestation than the peak splitting discussed above. Also, additional verification that the gate switching signal is not the cause of degraded peak shapes is found in the observation that the 50-μs modulation resolution HT-IMS spectrum in Figure 4a displays gate signal equal in intensity to the amphetamine peak, yet there is no splitting or broadening of the amphetamine peak. For the series of spectra in Figure 4, the ion peak intensities increase with longer modulation resolutions and at 150-μs all peaks, including the solvent peaks, are clearly resolved.

The resolving power in ion mobility is routinely measured by dividing the ion drift time by the width of the peak at half-height (fwhm).[28] The theoretical minimum fwhm calculated for IM separations of amphetamine for a 150-μs ion gate pulse width measured at atmospheric pressure with a 17.4 cm, 440 V/cm drift region operated at 175 °C is 180 μs,[27] which corresponds to a resolving power (R_P) of 75. A general trend of decreased R_P as the modulation resolution is increased is apparent for the HT-IMS spectra in Figure 4. An analogous inverse relationship between R_P and gate pulse width is also observed for SA-IMS spectra. The HT-IMS spectra obtained with a 150-μs modulation resolution is 295 μs (R_P = 45). In comparison, SA-IMS spectra collected with a 150-μs ion gate pulse width displayed nearly identical fwhm of 300 μs for the amphetamine peak. We interpret the similar resolving powers of the 150-μs SA-IMS and HT-IMS spectra as evidence that the HT-IMS modulation resolution is equivalent to the SA-IMS gate pulse width.

Effect of Pattern Sequence Length. Shown in Figure 5 are the HT-IMS amphetamine spectra acquired using Hadamard modulation sequences of various lengths ranging from S_{1023}, to S_{8191} with a 150-μs modulation resolution. The single sequence acquisition times are 150 ms for an S_{1023} modulation and 1.23 s for a S_{8191} modulation. The drift spectra in Figure 5 are deconvolutions of multiplexed ion signals collected as averages of 256 complete sequences for the S_{1023} and S_{2047} spectra (Figure 5a and b) and 128 sequences for the S_{4095} and S_{8191} spectra (Figure 5c and d). The significant differences in SNRs between the spectra are not due to differences in acquisition times as the S1023 spectrum corresponds to a 39-s acquisition time and no significant improvement in SNR was observed with additional sequence averaging. Notably, there is no substantial change in resolving power as a function of *m*-sequence length; however, the baseline noise varies greatly thereby affecting the SNR. Small baseline defects, e.g., at 12 ms in the S1023 and S2047 spectra and 23 ms in the S4095 spectrum, that are not present in the SA-IMS spectra appear in all the mobility spectra in Figure 5 except for the S8191 spectrum. The trend of increased SNR as a function of sequence length is expected for Hadamard-type modulations; 18 longer sequence lengths both distribute the experimental noise across a greater number of elements and attenuate baseline artifacts due to modulation defects. The S8191 transform produced the amphetamine spectra with the most favorable SNRs and was used for the following comparisons with traditional SA-IMS.

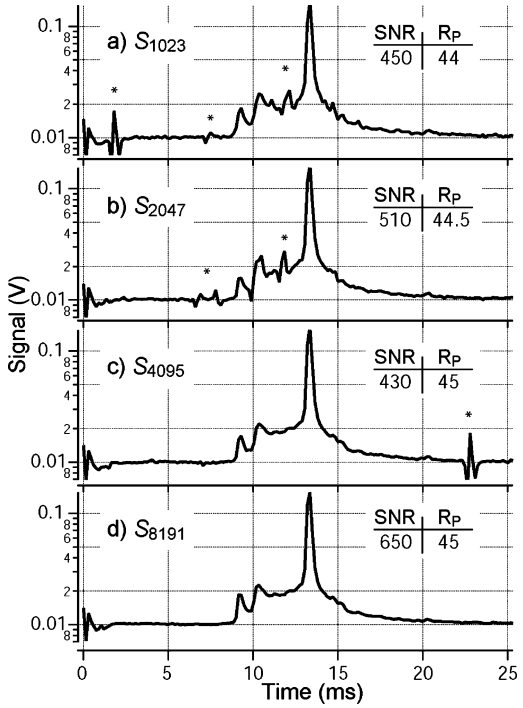

Figure 5. Influence of Hadamard *m*-sequence length on measured SNR. Spectra a−d correspond to 150-μs pulse width HT-IMS data acquired with *m*-sequences of lengths 1023, 2047, 4097, and 8191, respectively.

HT-IMS/SA-IMS Comparison. A direct comparison of HT-IMS and SA-IMS is best made by evaluating the SNRs and resolving powers of spectra acquired with equal total acquisition times and equal ion gate pulse widths. However, the SA-IMS spectra contain far more data points than HT-IMS spectra for the 25-ms drift time window of interest, 1000 points for SA-IMS versus 170 for HT-IMS. To ascertain how this might affect SNR and R_P comparisons, we first evaluated the effects of parsing a SA-IMS drift spectrum to obtain a spectrum with the same number of points as a HT-IMS spectrum. Equivalent SNRs and resolving powers were calculated for the original and parsed SA-IMS spectrum. Given this result, all HT-IMS/SA-IMS comparisons were made with SA-IMS data containing the full 1000 points/spectrum. Apart from the data acquisition electronics, the experimental conditions were kept identical for both SA-IMS and HT-IMS operations. As before, the SNR is calculated from the deconvoluted drift spectra as the baseline-corrected peak height divided by the standard deviation of the baseline region from 20 to 25 ms of the mobility spectrum.

The HT-IMS drift spectrum of amphetamine (20 ppm) in Figure 6a was acquired as an average of two sequences of a S_{8191} transform with a 150-μs modulation resolution and a total acquisition time of 2.46 s. In comparison, the SA-IMS drift spectrum collected with same amphetamine sample and a 2.45-s acquisition time, corresponding to an average of 98 drift spectra, is shown in Figure 6b. Although the amphetamine peak height is similar in

(28) Siems, W. F.; Wu, C.; Tarver, E. E.; Hill, H. H. Jr.; Larsen, P. R.; McMinn, D. G. *Anal. Chem.* **1994**, *66* (23), 4195−201.

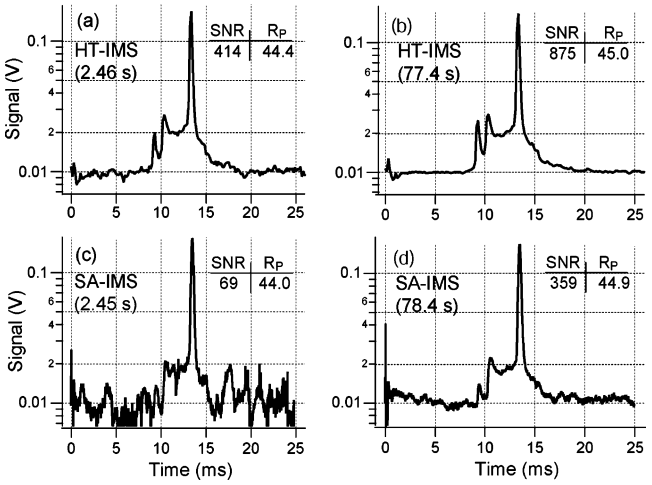

Figure 6. Comparison of the SNR of HT-IMS spectra a and b and SA-IMS spectra c and d. The spectra were acquired with 150-μs ion gate pulse width (SA) and S_{8191} transform with 150-μs modulation resolution (HT). The amphetamine spectra display similar resolving power at equivalent sampling times; however, the HT-IMS method demonstrates up to a 6-fold benefit in SNR for 25-ms drift spectra.

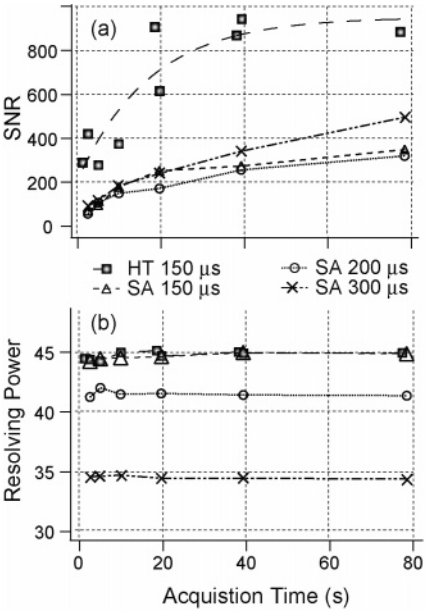

Figure 7. Comparison of SNR ratios and resolving powers as a function of data acquisition time for HT-IMS and SA-IMS amphetamine drift spectra. Plot a illustrates the increase in SNR provided by HT-IMS for all acquisition times. Plot b serves to show resolving power being maintained at a virtually constant level over the range of acquisition times.

both the SA-IMS and HT-IMS spectra, the baseline noise severely degrades the amphetamine SNR of the SA-IMS spectrum. The SNR of the HT-IMS amphetamine peak at 13.35 ms is 414 and represents a 6-fold increase compared to the SNR of 69 calculated for the equivalent SA-IMS amphetamine spectrum of Figure 6b. However, the amphetamine peak resolution is nearly identical for both the 150-μs modulation width HT-IMS (296 μs fwhm) and the 150-μs pulse width SA-IMS spectra (298 μs fwhm). A comparison of the SA-IMS and HT-IMS methods at longer sampling times (~78 s) is displayed in Figure 6b and d. The SNR advantage of the HT-IMS method is still observed at these extended sampling times. The SA-IMS spectrum shown in Figure 6d displays an amphetamine SNR of 359 that is 2.4 times smaller than that of the comparable HT-IMS spectrum (Figure 6b).

The SNRs and resolving powers calculated for both HT-IMS and SA-IMS amphetamine drift spectra are plotted in Figure 7 for acquisition times ranging from 1.23 to 78 s. The HT-IMS spectra are averages of 1−63 sequences of a 150-μs modulation resolution S_{8191} transform. While we note the importance of comparing spectra of equivalent gate pulse width and modulation resolution, we have included SA-IMS spectra with pulse widths of 150, 200, and 300 μs to provide a thorough comparison of the two techniques. The HT-IMS amphetamine SNR at each sampling time is substantially greater than that for the SA-IMS amphetamine spectra, regardless of the SA-IMS pulse width. The increased duty cycle of the longer pulse width SA-IMS spectra do result in higher SNRs than the 150-μs SA-IMS spectra; however, this is at the expense of reduced resolving power (Figure 7b). Notably, to match the SNR of 290 for a single 150-μs S_{8191} modulation (1.23-s acquisition time), an average of 1600 spectra in SA mode (a 40-s acquisition time) is required. The plot shown in Figure 7b illustrates that additional acquisition time does not significantly enhance the resolving power of either technique. The HT-IMS method offers a significant SNR enhancement over the standard SA-IMS technique with no reduction in resolving power.

The cytochrome *c* drift spectra in Figure 8 illustrate the increased benefits of HT acquisition when examining ions with extended drift times. Again, to accurately compare the HT and SA modes, equal times of acquisition were used for the spectra in Figure 8. The top trace (Figure 8a) represents the deconvolution of a two sequence average of a 150-μs, S_{32768} transform. Whereas, trace b of Figure 8 corresponds to the SA cytochrome *c* spectrum acquired with a gate pulse of 150 μs, and an equivalent 9.9-s sampling time. The best-fit lines of the peaks located within the electrospray charge envelope of cytochrome *c* are shown above each SA-IMS and HT-IMS spectrum. While the absolute peak intensity of the SA data set shown in Figure 8b is larger than the corresponding HT trace (Figure 8a), the SNR ratio favors the HT acquisition method. The average SNR for asterisk-labeled peaks in Figures 8a and b are 47 and 4.7, respectively. When compared to Figure 8b, the HT-IMS method offers the benefit of a 10-fold increase in SNR and moderate gains in resolving power. While the SNR for the SA data improved with increasing gate pulse width (data not shown), the resolving power of the measurement significantly decreased.

To understand why the benefits afforded by HT-IMS become more pronounced when examining larger ions such as cytochrome *c*, we need to revisit the nature of both HT and SA experimental modes. Compared to smaller ions (t_d < 25 ms), larger ions drift at slower rates and consequently diffuse greater distances. Since ions that occupy the fringe of the ion plume may discharge on the IMS drift rings, the increased radial diffusion length reduces the number of ions available for detection. To maintain adequate SNRs for SA-IMS measurements of low mobility ions such as cytochrome *c*, it is common to increase the ion gate pulse width to maintain signal intensity. Stated differently, to maintain the same level of signal intensity, the duty cycle of the experiment must be matched to that of a short time scale SA-IMS experiment, hence, an increase in ion gate pulse width when examining lower mobility ions. The SNR for the SA-IMS spectrum shown in Figure 8b may

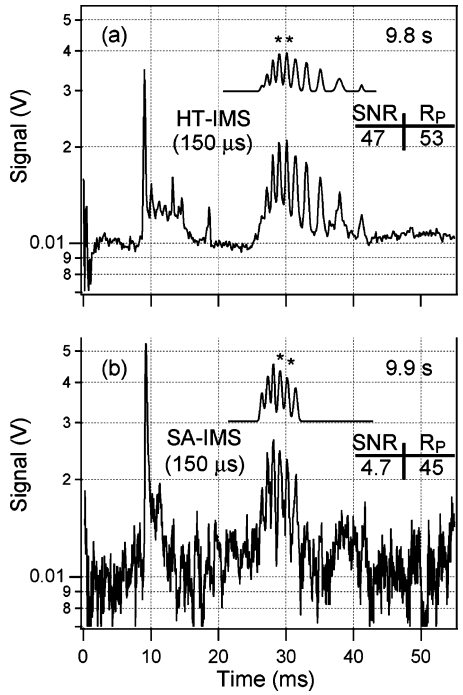

Figure 8. Comparison of the SA-IMS and HT-IMS spectra of cytochrome *c*. The upper spectrum corresponds to a two-sequence average of a 150-μs, S_{32767} HT-IMS spectrum of cytochrome *c* with the best fit of the charge envelope displayed above. The time equivalent SA-IMS spectrum of cytochrome *c* is shown in the lower trace with the best fit of the charge envelope elevated above the spectrum. The asterisk-labeled peaks located within the best fit traces were used for comparison. A 10-fold increase in SNR was observed for HT-IMS spectrum of cytochrome *c* when compared to the SA-IMS data.

be improved by increasing the ion gate pulse width; however, a loss of resolving power will ultimately result. While the limits of the experimental duty cycle severely hinder the ability of SA-IMS to examine larger ions, the HT-IMS mode of operation is not limited in this respect—HT-IMS can operate at a 50% duty cycle while maintaining spectral resolution across a wide range of ion drift times, up to the modulation time period (1.23 s, for a S_{8191} transform).

The theoretical maximum SNR gain attainable using Simplex-type modulations over traditional SA techniques is the square root of the number of elements in the sequence used to resolve a spectrum divided by 2.[23,24] Therefore, an *S* matrix containing 8191 elements would result in a theoretical maximum gain of ~45. This predicted SNR gain is derived for sparse spectra in situations where the modulation sequence length and rate is adjusted to equal to the time period of the deconvoluted spectrum. However, the B−N ion gate limits the HT-IMS modulation rate, and it is not possible to match the modulation period to the desired drift time scale. The HT-IMS data reported in this work suggest a maximum experimental SNR gain of 10; the disparity between the predicted and observed SNR gains may in part be attributed to the different resolutions of the A/D converters of the data acquisition cards for the SA experiments (16-bits) and the HT experiments (effectively 8-bits). Future modifications to the FPGA programming of the HT electronics will allow full 12-bit data transfers at acquisition rates appropriate for HT-IMS operation and are planned for the next generation of DSP electronics.

CONCLUSION

The first application of the Hadamard transform multiplexing method to IMS has demonstrated a marked increase in the overall duty cycle of the IMS experiment. This increased efficiency produced a 2−10-fold increase in the SNR for HT-IMS spectra over traditional SA-IMS techniques with no reduction in resolving power. Improved SNRs for the HT-IMS technique are realized at all acquisition times in this study. The SNR enhancements provided by HT-IMS show particular promise for mobility measurements of ions with extended drift times. The duty cycle gains inherent to the HT-IMS experiment combined with future HT signal multiplexing studies promise to enhance the current performance of IMS as an analytical technique.

ACKNOWLEDGMENT

This work was supported by the Air Force Office of Scientific Research, STTR contract F49620-03-C-0074 (S.M.M., Southwest Sciences, Inc.), and the NSF Integrative Graduate Education and Research Training (IGERT) grant under NSF grant DGE−9972817 (H.H.H., Washington State University).

Received for review April 11, 2005. Accepted October 25, 2005.

AC050615K